

# The Rossiter–McLaughlin effect in Exoplanet Research

Amaury H.M.J. Triaud

**Abstract** The Rossiter–McLaughlin effect occurs during a planet’s transit. It provides the main means of measuring the sky-projected spin–orbit angle between a planet’s orbital plane, and its host star’s equatorial plane. Observing the Rossiter–McLaughlin effect is now a near routine procedure. It is an important element in the orbital characterisation of transiting exoplanets. Measurements of the spin–orbit angle have revealed a surprising diversity, far from the placid, Kantian and Laplacian ideals, whereby planets form, and remain, on orbital planes coincident with their star’s equator. This chapter will review a short history of the Rossiter–McLaughlin effect, how it is modelled, and will summarise the current state of the field before describing other uses for a spectroscopic transit, and alternative methods of measuring the spin–orbit angle.

## Introduction

The Rossiter–McLaughlin effect is the detection of a planetary transit using spectroscopy. It appears as an anomalous radial-velocity variation happening over the Doppler reflex motion that an orbiting planet imparts on its rotating host star (Fig. 1). The shape of the Rossiter–McLaughlin effect contains information about the ratio of the sizes between the planet and its host star, the rotational speed of the star, the impact parameter and the angle  $\lambda$  (historically called  $\beta$ , where  $\beta = -\lambda$ ), which is the sky-projected spin–orbit angle.

The Rossiter–McLaughlin effect was first reported for an exoplanet, in the case of HD 209458 b, by [Queloz et al. \(2000\)](#). This effect takes its name from a pair of pa-

---

Amaury H.M.J. Triaud  
University of Birmingham, School of Physics & Astronomy, Edgbaston, B15 2TT, Birmingham, United Kingdom, e-mail: [A.Triaud@bham.ac.uk](mailto:A.Triaud@bham.ac.uk)  
University of Cambridge, Institute of Astronomy, Madingley Road, CB3 0HA, Cambridge, United Kingdom,

pers published jointly by Rossiter (1924) and McLaughlin (1924), although earlier mentions exist. Schlesinger (1910) interprets discrepant radial-velocities obtained during an eclipse correctly, and Holt (1893) theorised about it much earlier than 1924. Currently the most complete collection of planetary spin–orbit angles can be found on [TEPCAT](#)<sup>1</sup> (Southworth 2011). To date, the catalogue lists 181 measurements/analyses made on 109 planets.

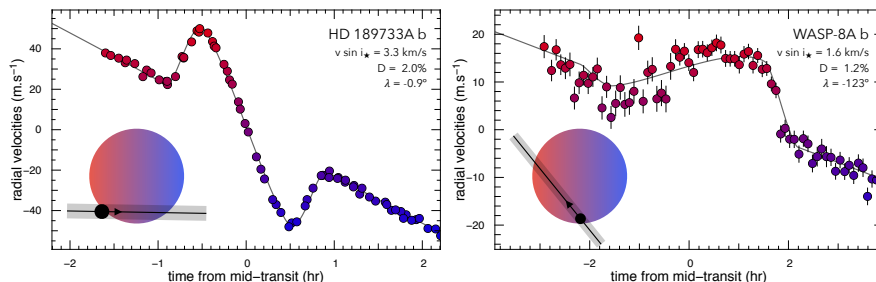


Fig. 1: The Rossiter–McLaughlin effect obtained on two transiting hot Jupiters, with the HARPS spectrograph. The left panel shows HD 189733A b, and on the right is plotted WASP-8A b. The radial-velocity measurements are colour-coded as a function of their Doppler information. The radial-velocity slope corresponds to the Doppler reflex motion of the host star, as caused by the orbiting planet. A most likely model is adjusted to the data, calculated from Giménez (2006a,b). Those measurements are reproduced from the analyses presented in Triaud et al. (2009) and Queloz et al. (2010) respectively. Visual representation of the orbits is provided on the bottom left of each panel.

Since Queloz et al. (2000), measuring the spin–orbit angle has become a staple of the orbital characterisation of planetary systems (e.g. Bouchy et al. 2005). Observations of the Rossiter–McLaughlin effect are now obtained routinely and provide observables able to inform a debate on the various migratory histories of exoplanets. The most astonishing result was the discovery that like for many other observables, exoplanets present a large diversity in their spin–orbit angle (e.g. Hébrard et al. 2008; Moutou et al. 2009; Johnson et al. 2009; Schlaufman 2010; Lendl et al. 2014; Anderson et al. 2015). Nearly a third of known hot Jupiters occupy orbits that are significantly misaligned with their host star (see Fig. 3, and Triaud et al. 2010; Winn and Fabrycky 2015), with many on retrograde orbits (e.g. Winn et al. 2009; Narita et al. 2009; Anderson et al. 2010; Queloz et al. 2010; Collier Cameron et al. 2010b; Addison et al. 2013; Esposito et al. 2014).

The distribution of  $\lambda$  (or rather, of  $|\lambda|$ ) with other (planetary or stellar) parameters can also be used to study the exchange of angular momentum between the planet and its host star, via tidal forces (e.g. Winn et al. 2010a; Triaud 2011b; Guil-

<sup>1</sup> [www.astro.keele.ac.uk/jkt/tepcat/](http://www.astro.keele.ac.uk/jkt/tepcat/)

lochon et al. 2011; Hébrard et al. 2011a; Brown et al. 2011; Albrecht et al. 2012; Dawson 2014; Petrovich 2015a; Anderson et al. 2015; Winn and Fabrycky 2015).

Our understanding of the Rossiter–McLaughlin effect has matured to a point where it can be used to confirm that an object is a planet, when RV precision is sufficient to rule out companion stars and brown dwarf, but too poor to enable the measure of a planetary mass (e.g. Collier Cameron et al. 2010b; Zhou et al. 2016b; Temple et al. 2017; Gaudi et al. 2017).

The Rossiter–McLaughlin effect can also be used to study the orbital inclination of eclipsing binary stars (its first application), and could be used to measure the rotational spin direction of exoplanets. It can provide information about an exoplanet’s atmospheric composition as well as be used in the context of exo-moons. Further descriptions of these can be found towards the back of the chapter. Before closing this chapter, we will also describe a few alternate methods that have been devised to estimate the projected spin–orbit angle, without requiring an observation of the Rossiter–McLaughlin effect. A few other techniques also provide related observables.

## Basic concept

A rotating star has one of its hemispheres blue-shifted and its other hemisphere red-shifted. This happens because one of its sides is approaching the observer while the other recedes. While the planet transits, it will cover different sections of the star sequentially. For instance, it can start to cover the blue-shifted side. In this case the average flux received by the observer will appear offset redward, creating a positive shift in the radial-velocity measured for the star, deviating from the Doppler reflex motion. As the planet scans the stellar velocity profile, the star appears to experience a rapid change in velocity. This is the Rossiter–McLaughlin effect (Fig. 1). A detailed introduction can be found in Gaudi and Winn (2007).

The shape of the Rossiter–McLaughlin effect contains several pieces of information. The most sought-after is that we can measure how long the planet spends over one hemisphere versus the other, which tells us the projected angle between the planet’s path and the stellar equator. As can be expected, to a first order, the semi-amplitude of the Rossiter–McLaughlin effect scales with the planet’s size and the stellar rotational velocity:

$$A_{\text{RM}} \simeq \frac{2}{3} D v \sin i_{\star} \sqrt{1 - b^2} \quad (1)$$

where  $D = (R_p/R_{\star})^2$  is the transit depth, relating  $R_p$  (the planet’s radius) to  $R_{\star}$  (the host star’s radius), where  $v$  is the rotational velocity of the star (at the equator),  $\sin i_{\star}$  is the inclination on the sky of the stellar rotation axis, and  $b$  is the impact parameter (in units of  $R_{\star}$ ). For a typical hot Jupiter with a transit depth of order 1.5%, and a typical star with a rotational velocity of  $2 \text{ km s}^{-1}$ , we obtain a semi-amplitude of order  $20 \text{ m s}^{-1}$ . The duration of the event is as long as the transit, which for a

hot Jupiter is often about two to three hours. The Rossiter–McLaughlin signal can be detected when collecting high-cadence radial-velocity measurements made with high-precision, stable, high-resolution spectrographs such as those routinely used in the search for exoplanets (see Fig. 1). Because the ingress and egress have a typical timescale of 20-30 minutes, a maximum recommended exposure for each spectrum is 10-15 minutes, but this can be adapted depending on the stellar and planetary parameters.

## Modelling the Rossiter–McLaughlin effect

### *The classical Rossiter–McLaughlin effect*

The earliest attempt to model the Rossiter–McLaughlin effect were made by [Petrie \(1938\)](#). At that time, the Rossiter–McLaughlin effect was referred to as the *rotation effect* (or *rotational effect*). The principal formulations were then made by [Kopal \(1942\)](#), but were only valid for coplanar systems. These calculations were generalised by [Hosokawa \(1953\)](#), who introduced the sky-projected spin–orbit angle<sup>2</sup> and called it  $\beta$ . Following this, a complete description was compiled by [Kopal \(1959, 1979\)](#). Kopal used  $\alpha$ -functions, based on Legendre polynomials to integrate over the visible surface of the stars. They can account for multiple distortions of the shape, and of the luminosity distribution. While flexible, this approach is not the easiest to follow, were computationally intensive (in the absence of modern computers). Simpler formulations are now available. In models elaborated for transiting exoplanets, only one uses Kopal’s formalism: [Giménez \(2006a,b\)](#).

Model adjustment on the first detection of the Rossiter–McLaughlin effect was made by drawing a grid over the star and reconstructing the cross correlation function of the stellar spectrum from which the radial-velocity is extracted ([Queloz et al. 2000](#)). A grid based approach is being used by a few authors (e.g. [Wittenmyer et al. 2005](#); [Covino et al. 2013](#); [Esposito et al. 2017](#)). This can be handy in some situations, notably when having to also treat various stellar effects, such as stellar variability due to spot-induced rotational modulation, or the overlap of spots by a transiting planet ([Oshagh et al. 2013, 2016](#)).

The notation most frequently used for the spin–orbit angle is  $\lambda$ , which was introduced in [Ohta et al. \(2005\)](#)<sup>3</sup>. This presents an analytical expression for the Rossiter–McLaughlin effect that has been widely used. Improvement on this formalism were made first by [Hirano et al. \(2011b\)](#), and by [Boué et al. \(2013\)](#), to resolve various issues related to different procedures used to extract radial velocities from stellar spectra. This can affect the amplitude and shape the radial-velocity anomaly that is the Rossiter–McLaughlin effect ([Triaud et al. 2009](#)). Please refer to [Boué et al.](#)

<sup>2</sup> for simplicity the sky-projected spin–orbit angle will often be referred to simply as the spin–orbit angle, within this document, something which is also done by several authors in the literature.

<sup>3</sup> with  $\lambda = -\beta$

(2013) for a more ample description. Recently a study compared several methods of analysis, and confirmed that the Boué model performs most consistently for instruments such as HARPS (Brown et al. 2017). Additional corrections can be made, for instance to account for a small bias in the spin–orbit angle created by ignoring stellar convective blue-shift (Shporer and Brown 2011). We caution here that not all stellar effects are accounted for in the modelling of the Rossiter–McLaughlin effect (Cegla et al. 2016b; Oshagh et al. 2016; Reiners et al. 2016).

For references on models of planetary transits, including the Rossiter–McLaughlin effect, please be directed to the chapter by Deeg, H., “Tools for Transit and Radial Velocity Modelling and Analysis” for additional information.

### *Some known pitfalls in model fitting*

Here are a few words of caution when attempting to adjust a model through the waveform of the Rossiter–McLaughlin effect.

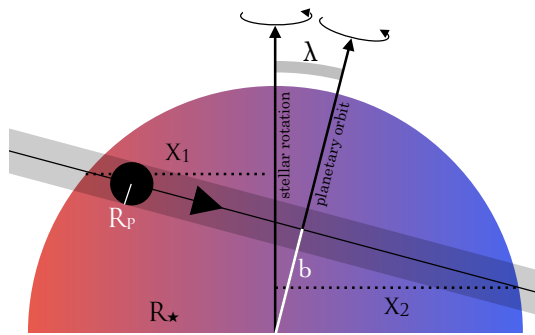


Fig. 2: Various quantities used to model the Rossiter–McLaughlin effect. Adapted from Fig. 1 in Albrecht et al. (2011b).

**When the impact parameter vanishes.** As the impact parameter  $b$  tends to zero, a degeneracy occurs between  $v \sin i_*$  and  $\lambda$ . This happens because in this instance, a heavily misaligned planet would produce a symmetrical effect: No matter how inclined the orbit is, the planet spends as much time on both hemispheres. A small  $\lambda$ , and low  $v \sin i_*$ , produce an equivalent effect to a high  $\lambda$ , high  $v \sin i_*$  when  $b = 0$ . This can be partially resolved if the stellar rotation is known and used as a prior (e.g. WASP-1 b, Albrecht et al. 2011b). However the stellar rotation as measured from spectral line broadening, and the values obtained from the Rossiter–McLaughlin effect are not always compatible (e.g. Triaud et al. 2011, 2015; Brown et al. 2017). An improper use of priors can also lead to spurious results as will be shown in the next paragraph.

What happens when  $b = 0$  has been detailed in [Albrecht et al. \(2011b\)](#) and is here reproduced. Let's define two distances,  $x_1$  and  $x_2$  (as show in Fig. 2), that can be shown to equate to:

$$\begin{aligned} x_1 &= \sqrt{1 - b^2} \cos \lambda - b \sin \lambda \\ x_2 &= \sqrt{1 - b^2} \cos \lambda + b \sin \lambda \end{aligned} \quad (2)$$

Following this we calculate the scaled sum of  $x_1$  and  $x_2$ :

$$\frac{1}{2} v \sin i_* (x_1 + x_2) = \sqrt{1 - b^2} v \sin i_* \cos \lambda, \quad (3)$$

and the scaled difference of  $x_1$  and  $x_2$ :

$$\frac{1}{2} v \sin i_* (x_1 - x_2) = b v \sin i_* \sin \lambda \quad (4)$$

Eq. 3 measures the semi-amplitude, and eq. 4 measures the asymmetry between both extrema. In eq. 4, we can see that when  $b = 0$ , the difference vanishes and we can only properly estimate the semi-amplitude, which is a function of  $v \sin i_*$  and  $\cos \lambda$ . For an extended discussion please refer to [Albrecht et al. \(2011b\)](#).

Because of this degeneracy, applying priors on  $v \sin i_*$  can lead to astonishing results: WASP-23 b is example with  $b \sim 0$ . Two different estimates of the stellar rotation were computed. Of both values, the faster rotation leads to a conclusion where WASP-23 b occupies a nearly perpendicular orbit to its host's equator, whereas the slower measurement of rotation makes  $\lambda$  compatible with an aligned solution ([Triaud et al. 2011](#)).

**Spin-orbit angles and non-detected effects.** If the star rotates, and if the planet transits, then there must be a Rossiter-McLaughlin effect in the spectroscopic data. However the effect is not always detected. Sometimes this is because of measurement uncertainties. At other times, the orbital configuration weakens the amplitude of the effect (e.g a situation close to  $b = 0$ ,  $\lambda = 90^\circ$ ). In both instances, good care must be taken.

A numerical experiment realised in [Albrecht et al. \(2011b\)](#) demonstrated that fitting for a Rossiter-McLaughlin effect through randomly distributed radial-velocity measurements (in the absence of a Rossiter-McLaughlin effect), leads to favoured angles around  $0^\circ$  and  $180^\circ$ . This is the main cause behind a faulty conclusion on WASP-2 b ([Triaud et al. 2010](#)). Initially the data was interpreted as showing evidence of a retrograde planet, but [Albrecht et al. \(2011b\)](#) convincingly showed that instead the event is not detected.

[Albrecht et al. \(2011b\)](#) also analysed WASP-1 b, and do not detect of the Rossiter-McLaughlin effect, but can conclude about its misalignment thanks to the high rotation rate of the star. Two similar cases with different outcomes.

**Combining parameters.** Usually, we know a planet transits before attempting Rossiter-McLaughlin observations. We already have precisely measured most of

the transit parameters. Fitting the Rossiter–McLaughlin effect essentially entails the adjustment of only two additional variables:  $v \sin i_*$  and  $\lambda$ . As  $v \sin i_*$  gets close to zero, or if  $v \sin i_*$  has a large uncertainty,  $\lambda$  becomes ill defined. Those two parameters are highly correlated in a non-linear way (as touched upon just above). This means that exploring parameter space can become inefficient when using Markov Chain Monte Carlo (MCMC) algorithms and can trick various optimisers into local minima. Furthermore, since a negative  $v \sin i_*$  is unphysical (although it could be interpreted as a retrograde planet), the value is often forced to remain positive. This can overestimate the detection significance of the Rossiter–McLaughlin effect.

If we examine eq. 3 & 4, we can notice that  $v \sin i_*$  and  $\lambda$  can be reparametrised into  $(v \sin i_* \cos \lambda)$  and  $(v \sin i_* \sin \lambda)$ . This is analogous to the orbital eccentricity  $e$ , which can be combined to its angle of periastron  $\omega$  into  $(e \cos \omega, e \sin \omega)$  (Ford 2005). However, as noted in Ford (2006), when sampling uniformly, this creates a prior that increases linearly with  $e$  instead of being un-informative. This biases  $e$  towards higher values, and led to a series of spurious detections of eccentricities for short-period hot Jupiters.

This also happened during the original analysis of WASP-2 b (in Triaud et al. 2010) and called upon by Albrecht et al. (2011b). In the case of eccentricity the problem was remedied by using instead  $(\sqrt{e} \cos \omega, \sqrt{e} \sin \omega)$ . A similar operation can be made for our parameters of interest:  $(\sqrt{v \sin i_*} \cos \lambda, \sqrt{v \sin i_*} \sin \lambda)$  (Triaud et al. 2011).

### *Alternate ways of modelling the Rossiter–McLaughlin effect*

**Doppler tomography.** The traditional way of modelling the Rossiter–McLaughlin effect is via a radial-velocity timeseries. The information contained in the radial-velocity originates from mis-shaped stellar absorption lines, caused by a deficit of flux on the blue or red-shifted hemisphere. It is challenging to detect temporal variations in the shape of a single line by a transiting planet, although it has been achieved for some eclipsing binaries (Albrecht et al. 2007, 2009). In the situation of a planet, this is solved by collecting multiple lines (and thousands exist in the wavelength range of most high-resolution spectrographs), sometimes in the form of a cross-correlation function. The study of a line shape is called Doppler tomography and has been used in a variety of applications, like mapping inhomogeneities on stellar surfaces, investigate magnetic fields, study binaries, and their accretion flows, but also planetary atmospheres, resolve planetary orbital motion, as well as reveal cloud patches in brown dwarf atmospheres (e.g. Marsh and Horne 1988; Richards et al. 1995; Collier Cameron 1998; Donati et al. 2006; Snellen et al. 2010; Rodler et al. 2012; Brogi et al. 2012; Crossfield et al. 2014; Richards et al. 2014).

The mean, out-of-transit, line shape is removed from all epochs. If a dark inhomogeneity exists on the stellar surface, it appears as a positive bump, that will appear at ingress, travel from one side of the line to the other side and disappear at egress. We call this signal the planet’s *trace*, or the planet’s *Doppler shadow*. This was

first done on HD 189733A b by [Collier Cameron et al. \(2010a\)](#), and the technique was quickly adopted to confirm WASP-33 b ([Collier Cameron et al. 2010b](#)). In this particular case the planet orbits a pulsating  $\delta$  Scuti, in a retrograde configuration. WASP-33 b’s Doppler shadow offers an angle, to the signal that stellar pulsations produce in the tomogram, and which rotate in and out of view in the direction of rotation.

Doppler tomography has now been adopted by several authors (e.g. [Brown et al. 2012b](#); [Gandolfi et al. 2012](#); [Albrecht et al. 2013](#); [Zhou et al. 2016a](#); [Temple et al. 2017](#)) and is most often used for faster rotating stars where the Doppler shadow is easier to resolve, and where radial-velocity uncertainties increase. The Doppler shadow is modelled with similar observables to those used for the Rossiter–McLaughlin effect. The planet’s bump also carries information about the stellar rotation. It was expected that  $v \sin i_*$  would be more accurately determined and that the model adjustment to the data would be less sensitive to degeneracies arising when the impact parameter approaches zero. However a comparison analysis did not show a clear preference for this approach ([Brown et al. 2017](#)). Of interest is that the planet trace forms a signal close to a line, which is a simpler shape to adjust a model to than the usual succession of three slopes seen on Fig. 1. Tomography can in principle be more forgiving about the observing cadence than the traditional Rossiter–McLaughlin effect would. Contrary to the Rossiter–McLaughlin effect, the Doppler shadow does not become 0 when the planet crosses the stellar axis, which can also help boost the significance of a detection and study configurations near  $\lambda = 90^\circ$  (e.g. WASP-76 b; [Brown et al. 2017](#)).

**The Rossiter–McLaughlin effect reloaded.** An additional method was recently devised. It relies on reconstructing the velocity field that the planet hides during transit, using line profiles (or cross correlation functions). A description can be found in [Cegla et al. \(2016a\)](#), where this method is applied on HD 189733A b. This new approach is ambitious and can recover the latitudinal differential rotation, the true axis of the star  $i_*$ , and account for convective blueshift and its centre to limb variation. Having measured  $i_*$  the authors could also compute  $\psi$ , the true spin–orbit angle, instead of  $\lambda$ ,  $\psi$ ’s sky-projection. There are also indications that spot-crossing events can be identified. A recent re-analysis of the WASP-8A b transit ([Bourrier et al. 2017](#)) yielded a spin–orbit significantly different to its original, traditional analysis ([Queloz et al. 2010](#)), although the planet remains retrograde.

## Measuring $\psi$

The traditional Rossiter–McLaughlin effect only provides information on sky-projected spin–orbit angle,  $\lambda$ . However, the true spin–orbit angle  $\psi$  is the quantity that is really sought after. Statistical comparison between theoretical  $\psi$  distributions (e.g. [Wu et al. 2007](#); [Fabrycky and Tremaine 2007](#); [Chatterjee et al. 2008](#); [Nagasawa et al. 2008](#); [Naoz et al. 2012](#); [Petrovich 2015a](#)) and the observed  $\lambda$  can be



made. This is done either by projecting  $\psi$  on the sky, or de-projecting  $\lambda$  (Fabrycky and Winn 2009; Triaud et al. 2010; Brown et al. 2012a). Fabrycky and Winn (2009) relate  $\psi$  to  $\lambda$ :

$$\cos \psi = \cos i_{\star} \cos i_p + \sin i_{\star} \sin i_p \cos \lambda \quad (5)$$

However, the best correction would be no correction at all. The key in estimating  $\psi$  lies in measuring  $i_{\star}$  properly, which is a hard measurement to make. There exist various ways but the most frequent is to transform a determination of the rotation period of the star (whose radius is often accurately known) into an equatorial velocity  $v$ , and solve for  $\sin i_{\star}$ . Complications arise because  $v \sin i_{\star}$  as measured via fitting the Rossiter–McLaughlin effect can differ from the value usually estimated from spectral line broadening (Triaud et al. 2011, 2015), and can be affected by latitudinal differential rotation. Moreover, determining the rotation period of a star can be fraught with uncertainties too. Stellar rotation is often measured by the photometric modulation caused by spots rotating in and out of view as the star rotates. Spots can be multiple, and located at different latitudes, providing different rotation periods. Empirical relations between activity levels and rotation period (e.g. Mamajek and Hillenbrand 2008) are also used, but their accuracy for single objects remain far from guaranteed. This has not prevented many authors to produce estimates of  $\psi$  (e.g. Winn et al. 2009; Hébrard et al. 2011b; Sanchis-Ojeda and Winn 2011; Hellier et al. 2011; Lendl et al. 2014; Anderson et al. 2015; Zhou et al. 2016b; Esposito et al. 2017). These attempts are very informative, but should be taken more critically than  $\lambda$ .

The most robust determination of  $\psi$  so far, was probably brought forward thanks to asteroseismology. Rotation induces a splitting of oscillation modes, that can be used to compute  $i_{\star}$  (Gizon and Solanki 2003). This has provided an alternative method to measuring the spin–orbit angle of a planetary orbit (see later; Chaplin et al. 2013; Huber et al. 2013; Van Eylen et al. 2014), but combined with the Rossiter–McLaughlin effect, this leads to  $\psi$  (Benomar et al. 2014; Campante et al. 2016).

## Rossiter-McLaughlin measurements on hot Jupiters

Apart from measurements on HAT-P-11 b, a near-polar Neptune-sized object (e.g. Winn et al. 2010b; Hirano et al. 2011a), an attempt on GJ 436 b, another Neptune (Albrecht et al. 2012), and two attempts on 55 Cnc e, a super-Earth (López-Morales et al. 2014; Bourrier and Hébrard 2014), the bulk of the observations have concentrated on gas giants, and particularly on hot Jupiters.

**Setting the scene.** Hot Jupiters are loosely defined. Typically, they are planets with masses in excess of  $0.1 M_{\text{Jup}}$ , and periods shorter than  $\sim 10$  days of which 51 Peg b is a good (and the first) example (Mayor and Queloz 1995) (for more information, please read the chapter by Santerne, A. “Hot Jupiter Populations from Transit and RV Surveys”. The population is identified by an over-density around a three day

orbital period, for a G dwarf host (e.g. [Santerne et al. 2016](#)). There is considerable debate on how hot Jupiters are formed.

Hot Jupiters could theoretically assemble on orbits close to those we observe them on ([Bodenheimer et al. 2000](#); [Batygin et al. 2015](#)). However the lack of nearby sub-Neptune companions to hot Jupiters contradicts this scenario ([Huang et al. 2016](#)). Only one hot Jupiter escapes this otherwise general rule: WASP-47 b ([Becker et al. 2015](#); [Neveu-VanMalle et al. 2016](#)). The situation is different for gas giants on orbits longer than 10 days, sometimes dubbed *warm Jupiters*. They exist frequently alongside close-by companions, which informs us that warm and hot Jupiters constitute two separate populations of gas giants. Those two populations probably overlap, and it is credible that WASP-47 b happens to be amongst the shortest orbiting examples of the warm population ([Huang et al. 2016](#)).

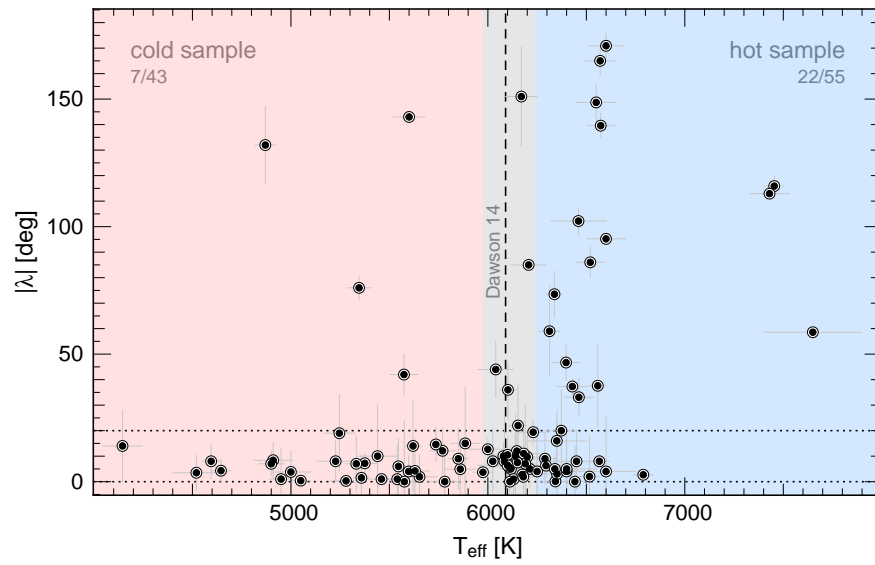


Fig. 3: Scatter plot showing the absolute values of the projected spin–orbit angles  $\lambda$  as a function of the host star’s effective temperature, for gas giants. A cold and a hot sample are separated by a transition effective temperature as determined by [Dawson \(2014\)](#). The most likely value (6090 K) is shown with a vertical dashed line, and the grey region around it is the  $1\sigma$  confidence region. The two dotted horizontal lines contain planets that can be considered on coplanar orbits. The numbers show the fraction of planets that are non-coplanar on either side of the dashed line. KELT9 b escapes this diagram on the right hand side (and is non-coplanar).

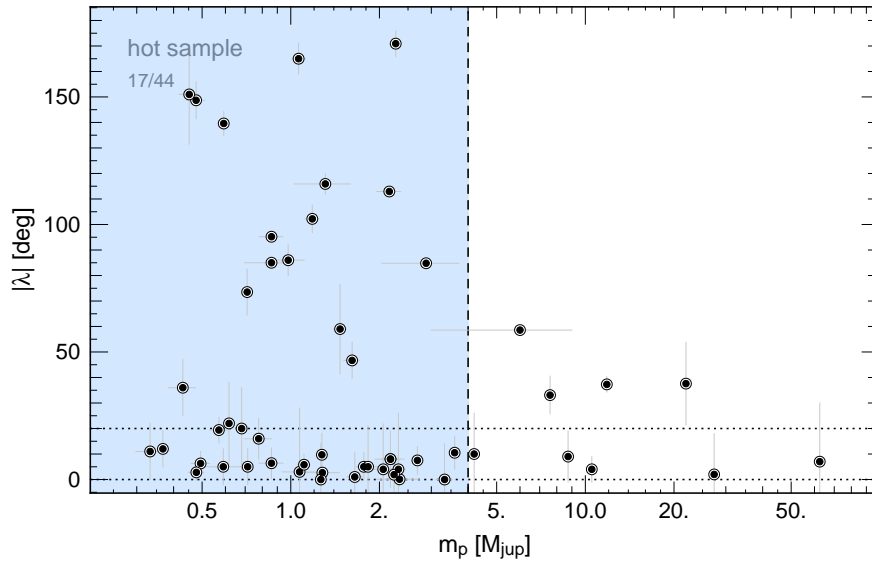


Fig. 4: Scatter plot showing the hot sample of  $\lambda$  values, defined in Fig. 3, and ordered against the planet’s mass. The two dotted horizontal lines contain planets that can be considered on coplanar orbits. A lack of retrograde planet was noticed by Hébrard et al. (2011b) and is visible here too, for masses  $> 3M_{\text{Jup}}$  (vertical dashed line). The number shows the fraction of planets that are non coplanar on the left hand side of the dashed line.

The alternative is that hot Jupiters form further from their star (e.g. Rafikov 2006), and migrate inwards. This orbital migration takes two main flavours: disc-driven migration, and disc-free migration.

Disc-driven migration is expected to keep gas giants within the plane of the disc as the planet exchanges angular momentum with the disc material to reduce its semi-major axis (Goldreich and Tremaine 1980; Lin et al. 1996; Ward 1997; Baruteau et al. 2014). If the whole disc is misaligned (Batygin 2012; Lai 2014) with the stellar equator (which is not observed; Greaves et al. 2014), or if the disc’s outer parts are warped (Terquem 2013), gas giants can end up on inclined orbits.

Disc-free migration contains a vast number of scenarios that come (so far) under one general umbrella: dynamical interactions placing a planet on an eccentric orbit, whose semimajor axis decays thanks to tidal dissipation when the planet is at periastron. This can be caused by other planets in the system (Rasio and Ford 1996; Nagasawa et al. 2008; Chatterjee et al. 2008; Wu and Lithwick 2011; Naoz et al. 2011; Petrovich 2015a), other stars (Wu et al. 2007; Fabrycky and Tremaine 2007; Malmberg et al. 2011; Naoz et al. 2012; Petrovich 2015b) or a disc (Terquem and Ajmia 2010; Terquem 2013).

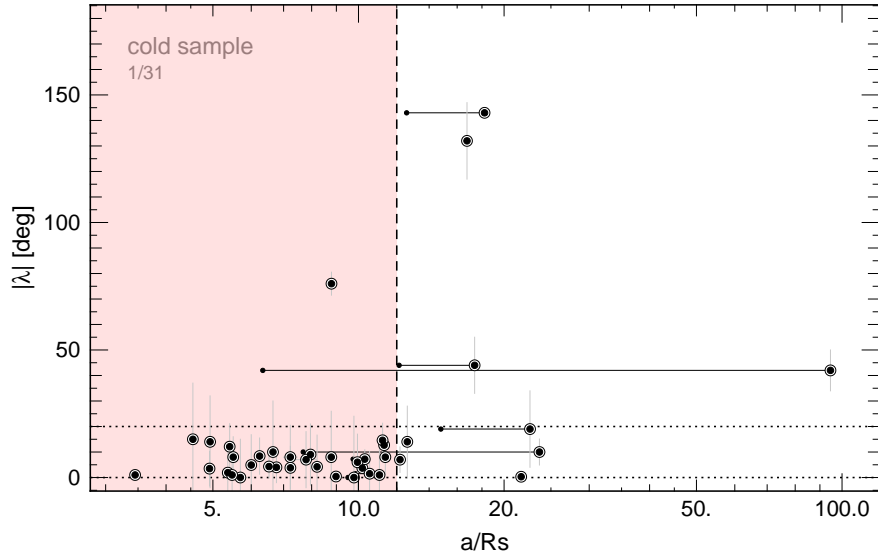


Fig. 5: Scatter plot showing the cold sample of  $\lambda$  values, defined in Fig. 3, and ordered versus the orbital separation in units of stellar radii ( $a/R_*$ ). Orbital eccentricities are depicted with a thin horizontal line ending with a dot, at the distance of periastron. The two dotted horizontal lines contain planets that can be considered on coplanar orbits. A lack of misaligned and circular orbits is seen for  $a/R_* < 12$  (vertical dashed line) (Anderson et al. 2015). The number shows the fraction of planets that are non coplanar on the left hand side of the vertical dashed line.

We could also imagine that the two processes can be mixed together, with planets getting closer to their star first by disc-driven accretion, which ceases but is followed by a disc-free, dynamical and tidal migration.

These multiple scenarios can produce both aligned and inclined planets making inferences hard to make. This is compounded by the fact that tides likely affect the distribution of spin-orbit angles, and that sometimes the stellar axis of rotation itself may not be stable. It might vary with respect to a planetary orbit, during the disc phase (Lai et al. 2011), or afterwards (Cébron et al. 2013; Rogers et al. 2013).

For a more rigorous discussion on planetary migration, the reader should consult the chapter by Nelson, R., “Planetary Migration in Protoplanetary Disks”.

**The measurements.** Fig. 3 to 6 represent the population as catalogued in TEP-CAT (2017-06-26). Only planets with masses  $> 0.1M_{\text{Jup}}$  are represented. A number of measurements have also been curated out on account of uncertain parameters, degenerate solutions, or concerns with the analysis. Spin-orbit angles  $\lambda$  with uncertainties greater than  $30^\circ$  are also discarded. This leaves 93 systems, 26 of which are misaligned, which are represented in Fig. 3. Those systems can be considered

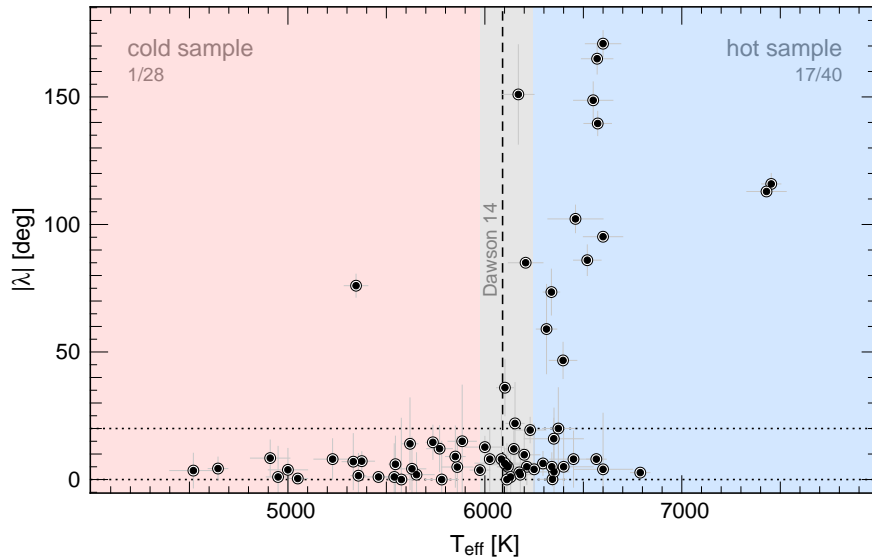


Fig. 6: Reproduction of Fig. 3 after the removal of patterns shown in Fig. 4 & 5. The cold and a hot sample are more contrasted than in Fig. 3. The two dotted horizontal lines contain planets that can be considered on coplanar orbits. The numbers show the fraction of planets that are non coplanar on either side of the dashed line.

as coming from two populations, a *cold* and a *hot* sample, separated at around  $T_{\text{eff}} = 6090^{+150}_{-110} \text{K}$  (Dawson 2014). The cold sample is typically formed of coplanar planets, whereas the hot sample contains a much larger occurrence of inclined orbits. This pattern was noticed by Schlafman (2010) and Winn et al. (2010a), and confirmed in Albrecht et al. (2012) and Brown et al. (2017). A likely interpretation is provided by Dawson (2014) and involves tides, as well as the spin-down of stars thanks to magnetic braking.

Scrutinising the cold and hot samples in isolation, they too come with patterns. Within the hot sample, we can observe that planets with masses above  $\sim 3M_{\text{Jup}}$  are less likely to be retrograde (Fig. 4; Hébrard et al. 2011b). This is understood to be because tidal realignment scales with  $(M_{\star}/m_{\text{p}})^2$  (Zahn 1977; Barker and Ogilvie 2009; Dawson 2014).

The cold sample is interesting too, if ordered as a function of the semimajor axis in units of stellar radii ( $a/R_{\star}$ ), which is a parameter directly determined from a transit lightcurve. For  $a/R_{\star} > 10 - 15$ , we observe a larger fraction of eccentric and of misaligned orbits. A first version of Fig. 5 is presented in Anderson et al. (2015). Here, the periastra are also represented with a horizontal line ending in a small dot showing that some of the planets with larger separations are likely on their way to become hot Jupiters (like HD 80606 b, the furthest to the right). This

pattern can emerge thanks to tides since the timescale of orbital realignment scales with  $(a/R_*)^6$  (Zahn 1977; Barker and Ogilvie 2009; Dawson 2014). It is also worth reflecting on the objects that are at large orbital separation, but are aligned. These gas giants are too far from their star for tides to be important in the evolution of their orbital parameters. WASP-84 b for instance, is circular, and aligned, at  $a/R_* > 20$  (Anderson et al. 2015). This means it is consistent with having formed locally in a coplanar protoplanetary disc, or that it followed a disc-driven migration.

Now that two additional patterns have been noticed in the hot and cold sample, we can do a final exercise and remove all planets with masses  $> 3M_{\text{Jup}}$  and  $a/R_* > 12$ , to obtain a *cleaned* version of Fig. 3 that is presented in Fig. 6. The contrast between the cold and hot sample is now reinforced (a similar route is taken in Albrecht et al. (2012)). The only misaligned object orbiting a cold star is HATS-14 b (Zhou et al. 2015).

**Lessons from the data.** More planets are coplanar than misaligned, and coplanarity becomes the norm for planets orbiting stars with  $T_{\text{eff}} < 6100$  on close, circular orbits. Patterns with planet mass, and planet separation are consistent with tidal realignment, but may also show different processes. For instance for  $a/R_* > 12$  we mostly have warm Jupiters instead of hot Jupiters, and both populations are different (Huang et al. 2016). If their formation, and/or orbital evolution are distinct, then the distribution in  $\lambda$  can be expected to be distinct too.

In order to learn about how hot Jupiters form we have to look in different ways. For instance, a different environment may provide different outcomes favouring one scenario over another. In open clusters, hot Jupiters appear more frequent (e.g. Brucalassi et al. 2016), which can be interpreted as a dynamical origin (e.g. Triaud 2016). Alternatively, the chemical make-up of transiting hot Jupiters can be retrieved thanks to transmission and emission spectroscopy (Deming and Seager 2017) (see Chapter by Kreidberg, L., “Exoplanet Atmosphere Observations from Transmission Spectroscopy and Other Planet-Star Combined Light Observational Techniques”). Different elemental abundances can be expected depending on the location of formation and the type of orbital migration (Öberg et al. 2011; Madhusudhan et al. 2011, 2017). This would also provide one additional way of comparing the hot to the warm Jupiters, but also the aligned to the misaligned planets (Huang et al. 2016).

## Alternate means to measure the spin–orbit angle of exoplanets

The Rossiter–McLaughlin effect and its derivatives are not the only means to measure an angle between a planet’s orbital plane and its host star’s equatorial plane. The success of Rossiter–McLaughlin effect observations and the surprising results it produced, catalysed a palette of other techniques able to extract the spin–orbit angle, or a related observable. This proves convenient to explore areas of parameter space

hard to reach with the traditional Rossiter–McLaughlin effect, or for stars that were too faint to conduct what remain fairly demanding and specialised observations.

**Using photometry.** Several methods were developed opportunistically, exploiting the availability of large, nearly un-interrupted photometric timeseries, of high quality acquired by the *Kepler* spacecraft. For instance, the shape of a planetary transit is controlled by the distribution of light covered by the passing planet. Fast rotating stars, instead of remaining spherical, become elliptical. The temperature is colder at the equator compared to the poles, with obvious effects on luminosity. This process is called gravity darkening, and distorts the standard transit shape (e.g. Barnes 2009), particularly if the orbit is misaligned with its star. This is how it was deduced that KOI-13.01 (now Kepler-13A b) occupies an inclined orbit (Szabó et al. 2011; Barnes et al. 2011). A recent analysis computes its true obliquity  $\psi$  by combining a tomographic measurement (Johnson et al. 2014) with gravity darkening (Masuda 2015).

*Kepler* also permitted a boom in asteroseismology. It provides a very elegant and robust way of measuring the inclination of the stellar axis with respect to sky. Oscillations in a star have typical frequencies notably dependent on their internal density. These frequencies are isolated by constructing a power spectrum of the photometric timeseries, where clear modes emerge from the noise (Chaplin and Miglio 2013). Fast rotation can split some of those modes. This has been realised for a transiting planet host for the first time by Chaplin et al. (2013), and led to the stunning result of two super-Earths coplanar with one another, but whose common plane is misaligned with the equator of their host, Kepler-56 (Huber et al. 2013).

Many Sun-like stars have spots. Spots create quasi-periodic modulations on a photometric timeseries, as they appear and disappear from the visible hemisphere, and as they evolve in size and latitude (e.g. Alonso et al. 2009). When a planet occults a spot, it also leaves a detectable imprint on its lightcurve (e.g. Pont et al. 2007). Particularly for stars rotating significantly slower than the planet’s orbital period, the spot will have moved a little by the time the planet returns in transit. An inclined planet will more easily miss the spot as it rotates out of the transit chord, but an aligned planet is likely to encounter the spot on a few occasions (Sanchis-Ojeda et al. 2011; Sanchis-Ojeda and Winn 2011; Nutzman et al. 2011; Mancini et al. 2014; Močnik et al. 2016; Dai et al. 2017). The timing of starspot crossings can also be combined with out-of-transit variations to estimate the spin–orbit angle (Sanchis-Ojeda et al. 2012). This is particularly effective when few spot crossing events are recorded, but does require a nearly continuous lightcurve.

**Resolving the orbital inclination of non-transiting planets.** Sahlmann et al. (2011) determine the orbital inclination of a planet on the sky using *Hipparcos* astrometry, boosting its signature thanks to radial-velocity data. This inclination appears inconsistent with the inclination of the stellar axis, measured by comparing the stellar  $v \sin i_*$ , and an activity indicator called  $\log R'_{\text{HK}}$ , which is correlated to stellar rotation periods (e.g. Mamajek and Hillenbrand 2008). This indicates the planet is likely misaligned.

When *GAIA* (Sozzetti, A., Bruijne, J., “Space Missions for Exoplanet Science with Gaia and the Legacy of HIPPARCOS”) makes its final data release, we ought to receive several thousand planetary orbits (e.g. Perryman et al. 2014) where this procedure can be reproduced. Those detections are expected to be gas giants, primarily, on orbital separation of a few AUs. They will provide a particularly interesting sample, in parts because we can compare it to the hot Jupiters. Some of these *GAIA* detections will happen in systems where close-in planets are (or will become) known to transit, while remaining undetected astrometrically. Then we can be in a position to collect information on mutual inclinations (Triaud et al. 2017b) and therefore on the spin–orbit alignment of distant planets. Similarly, it will become possible to measure the inclination between the orbital plane of a circumbinary planet and the plane of its central binary (Sahlmann et al. 2015)

Using CRILES, Rodler et al. (2012) and Brogi et al. (2012) resolved the planet  $\tau$  Boötis b spectroscopically, and could measure its orbital inclination on the sky and therefore, its true mass. Adopting this inclination for the star, its  $v \sin i_*$  yields a rotation period consistent with the planet’s orbital period, indicative of having achieved tidal synchronisation, as was proposed by Donati et al. (2008) based on Zeeman Doppler Imaging data. This strongly suggests that  $\tau$  Boo b is coplanar with its star, in line with the general behaviour of massive planets (Hébrard et al. 2011a).

**Dynamical effects.** The orbital inclination of circumbinary planets such as Kepler-16 b (Doyle et al. 2011) is accurately known from the photometry, as the planet transits first one star and then the other, and does so again at every orbital period. However, if the planet is but a little inclined with respect to the binary orbital plane, it will torque the planetary orbit causing it to precess or nutate (e.g. Doolin and Blundell 2011). This will move the planet in and out of *transitability* (Schneider 1994; Martin and Triaud 2014). The most inclined circumbinary planet is Kepler-413 b (Kostov et al. 2014), with an inclination of  $2.5^\circ$ .

On a similar note, a star rendered elliptical by its fast rotation will exert a torque on a planetary orbit, changing its transit chord in a noticeable manner as described in Szabó et al. (2011), Barnes et al. (2011), Johnson et al. (2015) and Masuda (2015). The period precession encodes information on the inclination of the planet with respect to the star.

**Statistically.** Most of these alternate methods work with observations obtained on singular systems. However it is also possible to approach the problem by examining the statistical properties of a given sample. Schlafman (2010) became the first to suggest a relation between spin–orbit misalignment and a stellar property, but did so without obtaining any observations of the Rossiter–McLaughlin effect. The conclusions were reached by noticing that a number of hosts ( $> 1.2M_\odot$ ) of transiting hot Jupiters have a rotation rate abnormally lower than the general stellar population. This shows that the stellar axis must be preferentially inclined. A similar method is employed by Mazeh et al. (2015) using the amplitude of photometric modulations acquired by *Kepler*, to argue that all planet-hosts (to hot Jupiters and other planet types) with  $T_{\text{eff}} > 6100\text{K}$  have rotation axes inclined with respect to our line of sight, and therefore, to the orbital plane of their transiting companions.



**The alignment of discs.** Finally, beyond planets, it is of obvious high interest to measure the spin–orbit angle between a star and any material surrounding it, like a debris or a protoplanetary disc. Resolving the stellar surface interferometrically, [Le Bouquin et al. \(2009\)](#) find an alignment between Fomalhaut and its debris ring.

A collection of debris discs, resolved by *Herschel*, show general agreement with discs being coplanar with the inferred inclination for their central star ([Watson et al. 2011](#); [Greaves et al. 2014](#)). We will note here the existence of one polar disc surrounding the circumbinary system 99 Herculis ([Kennedy et al. 2012](#)), and the presence of a warped disc in KH 15D ([Chiang and Murray-Clay 2004](#); [Winn et al. 2006](#)).

Misalignments appear more frequent in protoplanetary discs, with large mutual inclinations reported between two circumstellar discs surrounding each component of a binary system ([Jensen and Akeson 2014](#)), as well as between circumstellar and circumbinary discs ([Brinch et al. 2016](#)). Those however are generally consistent with stellar axes being unrelated to their orbital plane, for separations in excess of 30–40 AU ([Hale 1994](#)).

## Other uses for the Rossiter-McLaughlin effect

**Stellar binaries.** The Rossiter–McLaughlin effect was devised for binaries prior to its application to planets. However, beyond the 1940s, very few measurements have been obtained. The effect is perceived as a nuisance and generally observers avoid observing close to eclipses.

The fast growth of planetary measurement triggered a regain of interest, with the most striking result presented by [Albrecht et al. \(2009\)](#), who presented evidence that DI Herculis, a binary system, contains two stars, each with a spin misaligned with their orbital spin.

There are two main projects working along these lines of enquiry. While the BANANA project focuses on near equal mass, high-mass binaries ([Albrecht et al. 2011a](#)), the EBLM project ([Triaud et al. 2013, 2017a](#)) is concerned with unequal pairs, composed of FGK primaries with secondaries that have masses  $< 0.3M_{\odot}$ . These low mass stars have radii and effective temperatures comparable to many hot Jupiters ([Triaud 2014](#)). They mimic a transit of a Jupiter-sized planet exactly. As such they provide a natural comparison sample to the hot Jupiter population, amongst others for the measure of the Rossiter–McLaughlin effect ([Triaud et al. 2013](#)). A similar observation was carried out to verify that Kepler-16B orbits coplanar with Kepler-16A’s equator ([Winn et al. 2011](#)). This matches the coplanarity of the circumbinary planet Kepler-16AB b ([Doyle et al. 2011](#)).

**Exomoons.** An exomoon has yet to be discovered (see chapter by Heller, R. “Detecting and Characterizing Exomoons and Exorings”). However, the ubiquity of moons in the Solar system indicates that this is probably only a matter of time. [Zhuang et al. \(2012\)](#) provide a first analysis on what type of a Rossiter–McLaughlin effect should be expected while a moon transits a star, following its companion

planet. They show that multiple events can yield the orbital inclination of the moon to the planet's orbital plane.

Another method is likely possible, following the recent successes at resolving planets spectroscopically either from their reflected or their emission spectrum. [Snellen et al. \(2014\)](#) not only resolve  $\beta$  Pictoris b, but also measure its  $v \sin i_p$ . For comparable rotation rates to a star, an exomoon the size of the Earth would cast a Rossiter–McLaughlin effect with an amplitude similar to a hot Jupiter transiting a Sun-like star. Other alternative methods such as Doppler tomography are also available and are probably preferable.

**Planetary spin.** While the planetary orbital spin may be aligned with the stellar rotation spin, this may not necessarily be the case for the planetary spin (e.g. the Earth, whose spin is inclined by  $\sim 23.4^\circ$  compared to its orbital plane, giving rise to seasonal variations). At occultation, we can reconstruct the reflected and emitted spectrum of a planet. As the planet disappears behind the star, parts of its surface are scanned, and the spin–orbit angle of the planet to its orbit can in principle be measured although none have been reported so far ([Nikolov and Sainsbury-Martinez 2015](#)).

**Atmospheric investigations.** Opacity sources within a planetary atmosphere (atoms, molecules, particles) lead to a variation in apparent size of the planet, which is observed as a variation of the transit depth, as a function of wavelength ([Seager and Deming 2010](#)). Following equation 1 but replacing  $D$  by  $\Delta D$ , a change in transit depth, we can see that those would lead to a variation of the amplitude of the Rossiter–McLaughlin effect. This was first proposed, and applied by [Snellen \(2004\)](#) who confirmed an enhanced Rossiter–McLaughlin effect on the Sodium D lines for HD 209458 b. This has also been observed in the case of WASP-17 b ([Wood et al. 2011](#)), and recently [Di Gloria et al. \(2015\)](#) reported a marginal detection of the scattering slope of HD 189733 b. For these atmospheric observation, the Rossiter–McLaughlin effect has to be taken into account to obtain proper results ([Louden and Wheatley 2015](#); [Brogi et al. 2016](#); [Wytenbach et al. 2017](#)).

An important aspect is that  $v \sin i_*$  acts as an amplifier of atmospheric features. For instance, would TRAPPIST-1 b ([Gillon et al. 2016, 2017](#)) have a hydrogen-rich atmospheres (which it does not; [de Wit et al. 2016](#)), spectral features would be expected to cause Rossiter–McLaughlin amplitude variations of several metres per second thanks to the high spin rate of its host ([Cloutier and Triaud 2016](#)).

**Differential rotation.** Like a photometric transit, the Rossiter–McLaughlin effect can be used to study the star itself. At a near polar orbit, an exoplanet will scan different stellar latitudes. Latitudinal differential rotation will affect the shape of the Rossiter–McLaughlin effect. Although this effect was deemed too weak (e.g. [Triaud et al. 2009](#)) to be detected, the development of the *reloaded* method allowed a detection on HD 189733 ([Cegla et al. 2016a](#)). This opens a new chapter of investigations.

**Transit identification.** Identifying that a planet is transiting is not always straightforward. The transit can last a time comparable to a night, or the star can be so bright it has no reference star within the field of view of a ground-based telescope. In those

instances the Rossiter–McLaughlin effect can help make a detection. Such an observation was carried out on HD 80606 b (although it was accompanied by a photometric timeseries (Moutou et al. 2009) (read also Chapt. by F. Bouchy HD189733b: The transiting hot Jupiter that revealed a hazy and cloudy atmosphere, Bouchy et al. 2005). This also provided some of the first hints of significant spin–orbit misalignment, which was later confirmed in Hébrard et al. (2010). Another similar attempt was produced in the case of HD 156846 b, a 360d, eccentric planet. The HARPS measurements show no evidence of a transit, but these data were only presented in a thesis (Triaud 2011a).

Some planets will have a Rossiter–McLaughlin effect with an amplitude higher than its Doppler reflex motion. A careful analysis of residuals during transit can reveal that the planet is transiting straight away. This might become relevant for Doppler surveys of rapidly rotating late M-dwarfs (Cloutier and Triaud 2016).

**The Rossiter-McLaughlin effect on the Sun.** During the last transit of Venus, Molaro et al. (2013) used HARPS to recover a Rossiter–McLaughlin effect, from Sun light reflected off the Moon. These observations were carried out with the intent of replicating conditions close to what happens when collecting photons from a distant star while an exoplanet transits. The effect is tiny with a semi-amplitude of just  $1 \text{ m s}^{-1}$  (Molaro et al. 2013). They demonstrate that in principle, signals as weak as this can be properly recovered, with currently available technology.

The Rossiter–McLaughlin effect has also been captured during lunar eclipse, using HARPS (Yan et al. 2015), and using a solar telescope and a Fourier transform spectrograph (Reiners et al. 2016). The effect is stunning with a whopping  $1.4 \text{ km s}^{-1}$  total amplitude. These type of observations can be used as a benchmark to investigate multiple stellar effects, notably convective blue-shift and the modelling of centre-to-limb darkening.

## Conclusions

In the past ten years, we have discovered that the measure of the spin–orbit angle  $\lambda$  does not provide the clean diagnostics for planetary migration that we had been hoping for. Instead Nature has shown many surprises. These make the interpretation of the spin–orbit distribution challenging, but also, so very interesting. The measure of the spin–orbit angle, like for many other observable quantities, participates in building a context for each planet.

The future is bright. The first attempts to determine the spin–orbit angle of a super-Earth have been made (55 Cnc e; López-Morales et al. 2014; Bourrier and Hébrard 2014). They offer different conclusions but those should soon be resolved by up-coming instrument like ESPRESSO, on the VLT (see Gonzalez-Hernandez, J., Pepe, F., Molaro, P., Santos, N., “ESPRESSO on VLT: An Instrument for Exoplanet Research”). High on the agenda is to measure the angle for multiplanetary systems

orbiting stars with effective temperatures greater than 6100K, and verify the results provided by [Mazeh et al. \(2015\)](#). They indicate that super-Earths ought to be found on inclined orbits, supporting the idea that the more massive stars have unstable stellar axes. As TESS (see chapter by see Ricker, G., “Space Missions for Exoplanet Science: TESS”, and [Sullivan et al. 2015](#)) and PLATO (see chapter by Heras, A., Rauer, H., “Space Missions for Exoplanet Science: PLATO”, and [Rauer et al. 2014](#)) provide a large sample of super-Earths transiting relatively bright stars, we will have many investigations to carry out.

High-resolution spectrographs are being used more and more regularly for the study of planetary atmospheres, using ground-based facilities. Those observations are obtained at transit and contain the Rossiter–McLaughlin effect. There are two scientific uses for a same observation. Atmospheric work often required multiple epochs to build up the signal or quantify astrophysical systematics. We will gain a chance to improve the precision we obtain on  $\lambda$  and verify that epoch upon epoch provides reproducible results, an important element of the scientific method.

**Acknowledgements** The author would like to acknowledge the many discussions with friends, colleagues, collaborators and competitors that across the years have shaped my thoughts. Notably amongst them are: Simon Albrecht, David Anderson, Adrian Barker, Vincent Bourrier, David Brown, Heather Cegla, Andrew Collier Cameron, Bekki Dawson, Dan Fabrycky, Guillaume Hébrard, Dong Lai, Doug Lin, Claire Moutou, Soko Matsumura, Michel Mayor, Norio Narita, Smadar Naoz, Gordon Ogilvie, Cristobal Petrovich, Didier Queloz, Joshua Winn and Yanqin Wu. Finally, the author would like to thank Alexander von Boetticher for proof reading the document, and Roi Alonso for the opportunity to write this chapter.

## References

- Addison BC, Tinney CG, Wright DJ et al. (2013) A Nearly Polar Orbit for the Extrasolar Hot Jupiter WASP-79b. *ApJ*774:L9
- Albrecht S, Reffert S, Snellen I, Quirrenbach A Mitchell DS (2007) The spin axes orbital alignment of both stars within the eclipsing binary system V1143 Cyg using the Rossiter-McLaughlin effect. *A&A*474:565–573
- Albrecht S, Reffert S, Snellen IAG Winn JN (2009) Misaligned spin and orbital axes cause the anomalous precession of DIHerculis. *Nature*461:373–376
- Albrecht S, Winn JN, Carter JA, Snellen IAG de Mooij EJW (2011a) The Banana Project. III. Spin-Orbit Alignment in the Long-period Eclipsing Binary NY Cephei. *ApJ*726:68
- Albrecht S, Winn JN, Johnson JA et al. (2011b) Two Upper Limits on the Rossiter-McLaughlin Effect, with Differing Implications: WASP-1 has a High Obliquity and WASP-2 is Indeterminate. *ApJ*738:50
- Albrecht S, Winn JN, Johnson JA et al. (2012) Obliquities of Hot Jupiter Host Stars: Evidence for Tidal Interactions and Primordial Misalignments. *ApJ*757:18
- Albrecht S, Winn JN, Marcy GW et al. (2013) Low Stellar Obliquities in Compact Multiplanet Systems. *ApJ*771:11
- Alonso R, Guillot T, Mazeh T et al. (2009) The secondary eclipse of the transiting exoplanet CoRoT-2b. *A&A*501:L23–L26
- Anderson DR, Hellier C, Gillon M et al. (2010) Wasp-17b: An Ultra-Low Density Planet in a Probable Retrograde Orbit. *ApJ*709:159–167

- Anderson DR, Triaud AHMJ, Turner OD et al. (2015) The Well-aligned Orbit of Wasp-84b: Evidence for Disk Migration of a Hot Jupiter. *ApJ*800:L9
- Barker AJ, Ogilvie GI (2009) On the tidal evolution of Hot Jupiters on inclined orbits. *MNRAS*395:2268–2287
- Barnes JW (2009) Transit Lightcurves of Extrasolar Planets Orbiting Rapidly Rotating Stars. *ApJ*705:683–692
- Barnes JW, Linscott E, Shporer A (2011) Measurement of the Spin-Orbit Misalignment of KOI-13.01 from Its Gravity-darkened Kepler Transit Lightcurve. *ApJS*197:10
- Baruteau C, Crida A, Paardekooper SJ et al. (2014) Planet-Disk Interactions and Early Evolution of Planetary Systems. *Protostars and Planets VI* pp 667–689
- Batygin K (2012) A primordial origin for misalignments between stellar spin axes and planetary orbits. *Nature*491:418–420
- Batygin K, Bodenheimer PH, Laughlin GP (2015) In Situ Formation and Dynamical Evolution of Hot Jupiter Systems. *ArXiv e-prints*
- Becker JC, Vanderburg A, Adams FC, Rappaport SA, Schwengeler HM (2015) WASP-47: A Hot Jupiter System with Two Additional Planets Discovered by K2. *ApJ*812:L18
- Benomar O, Masuda K, Shibahashi H, Suto Y (2014) Determination of three-dimensional spin-orbit angle with joint analysis of asteroseismology, transit lightcurve, and the Rossiter-McLaughlin effect: Cases of HAT-P-7 and Kepler-25. *PASJ*66:94
- Bodenheimer P, Hubickyj O, Lissauer JJ (2000) Models of the in Situ Formation of Detected Extrasolar Giant Planets. *Icarus*143:2–14
- Bouchy F, Udry S, Mayor M et al. (2005) ELODIE metallicity-biased search for transiting Hot Jupiters. II. A very hot Jupiter transiting the bright K star HD 189733. *A&A*444:L15–L19
- Boué G, Montalto M, Boisse I, Oshagh M, Santos NC (2013) New analytical expressions of the Rossiter-McLaughlin effect adapted to different observation techniques. *A&A*550:A53
- Bourrier V, Hébrard G (2014) Detecting the spin-orbit misalignment of the super-Earth 55 Cancri e. *A&A*569:A65
- Bourrier V, Cegla HM, Lovis C, Wyttenbach A (2017) Refined architecture of the WASP-8 system: A cautionary tale for traditional Rossiter-McLaughlin analysis. *A&A*599:A33
- Brinch C, Jørgensen JK, Hogerheijde MR, Nelson RP, Gressel O (2016) Misaligned Disks in the Binary Protostar IRS 43. *ApJ*830:L16
- Brogi M, Snellen IAG, de Kok RJ et al. (2012) The signature of orbital motion from the dayside of the planet  $\tau$  Boötis b. *Nature*486:502–504
- Brogi M, de Kok RJ, Albrecht S et al. (2016) Rotation and Winds of Exoplanet HD 189733 b Measured with High-dispersion Transmission Spectroscopy. *ApJ*817:106
- Brown DJA, Collier Cameron A, Hall C, Hebb L, Smalley B (2011) Are falling planets spinning up their host stars? *MNRAS*415:605–618
- Brown DJA, Cameron AC, Anderson DR et al. (2012a) Rossiter-McLaughlin effect measurements for WASP-16, WASP-25 and WASP-31. *MNRAS*423:1503–1520
- Brown DJA, Collier Cameron A, Díaz RF et al. (2012b) Analysis of Spin-Orbit Alignment in the WASP-32, WASP-38, and HAT-P-27/WASP-40 Systems. *ApJ*760:139
- Brown DJA, Triaud AHMJ, Doyle AP et al. (2017) Rossiter-McLaughlin models and their effect on estimates of stellar rotation, illustrated using six WASP systems. *MNRAS*464:810–839
- Brucalassi A, Pasquini L, Saglia R et al. (2016) Search for giant planets in M67. III. Excess of hot Jupiters in dense open clusters. *A&A*592:L1
- Campante TL, Lund MN, Kuszewicz JS et al. (2016) Spin-Orbit Alignment of Exoplanet Systems: Ensemble Analysis Using Asteroseismology. *ApJ*819:85
- Cébron D, Bars ML, Gal PL et al. (2013) Elliptical instability in hot Jupiter systems. *Icarus*226:1642–1653
- Cegla HM, Lovis C, Bourrier V et al. (2016a) The Rossiter-McLaughlin effect reloaded: Probing the 3D spin-orbit geometry, differential stellar rotation, and the spatially-resolved stellar spectrum of star-planet systems. *ArXiv e-prints*
- Cegla HM, Oshagh M, Watson CA et al. (2016b) Modeling the Rossiter-McLaughlin Effect: Impact of the Convective Center-to-limb Variations in the Stellar Photosphere. *ApJ*819:67

- Chaplin WJ Miglio A (2013) Asteroseismology of Solar-Type and Red-Giant Stars. *ARA&A*51:353–392
- Chaplin WJ, Sanchis-Ojeda R, Campante TL et al. (2013) Asteroseismic Determination of Obliquities of the Exoplanet Systems Kepler-50 and Kepler-65. *ApJ*766:101
- Chatterjee S, Ford EB, Matsumura S Rasio FA (2008) Dynamical Outcomes of Planet-Planet Scattering. *ApJ*686:580–602
- Chiang EI Murray-Clay RA (2004) The Circumbinary Ring of KH 15D. *ApJ*607:913–920
- Cloutier R Triaud AHMJ (2016) Prospects for detecting the Rossiter-McLaughlin effect of Earth-like planets: the test case of TRAPPIST-1b and c. *MNRAS*462:4018–4027
- Collier Cameron A (1998) Stellar Tomography. *Ap&SS*261:71–80
- Collier Cameron A, Bruce VA, Miller GRM, Triaud AHMJ Queloz D (2010a) Line-profile tomography of exoplanet transits - I. The Doppler shadow of HD 189733b. *MNRAS*403:151–158
- Collier Cameron A, Guenther E, Smalley B et al. (2010b) Line-profile tomography of exoplanet transits - II. A gas-giant planet transiting a rapidly rotating A5 star. *MNRAS*407:507–514
- Covino E, Esposito M, Barbieri M et al. (2013) The GAPS programme with HARPS-N at TNG. I. Observations of the Rossiter-McLaughlin effect and characterisation of the transiting system Qatar-1. *A&A*554:A28
- Crossfield IJM, Biller B, Schlieder JE et al. (2014) A global cloud map of the nearest known brown dwarf. *Nature*505:654–656
- Dai F, Winn JN, Yu L Albrecht S (2017) The Stellar Obliquity, Planet Mass, and Very Low Albedo of Qatar-2 from K2 Photometry. *AJ*153:40
- Dawson RI (2014) On the Tidal Origin of Hot Jupiter Stellar Obliquity Trends. *ApJ*790:L31
- de Wit J, Wakeford HR, Gillon M et al. (2016) A combined transmission spectrum of the Earth-sized exoplanets TRAPPIST-1 b and c. *Nature*537:69–72
- Deming LD Seager S (2017) Illusion and reality in the atmospheres of exoplanets. *Journal of Geophysical Research (Planets)* 122:53–75
- Di Gloria E, Snellen IAG Albrecht S (2015) Using the chromatic Rossiter-McLaughlin effect to probe the broadband signature in the optical transmission spectrum of HD 189733b. *A&A*580:A84
- Donati JF, Forveille T, Collier Cameron A et al. (2006) The Large-Scale Axisymmetric Magnetic Topology of a Very-Low-Mass Fully Convective Star. *Science* 311:633–635
- Donati JF, Moutou C, Farès R et al. (2008) Magnetic cycles of the planet-hosting star  $\tau$  Bootis. *MNRAS*385:1179–1185
- Doolin S Blundell KM (2011) The dynamics and stability of circumbinary orbits. *MNRAS*418:2656–2668
- Doyle LR, Carter JA, Fabrycky DC et al. (2011) Kepler-16: A Transiting Circumbinary Planet. *Science* 333:1602–
- Esposito M, Covino E, Mancini L et al. (2014) The GAPS Programme with HARPS-N at TNG. III: The retrograde orbit of HAT-P-18b. *A&A*564:L13
- Esposito M, Covino E, Desidera S et al. (2017) The GAPS Programme with HARPS-N at TNG. XIII. The orbital obliquity of three close-in massive planets hosted by dwarf K-type stars: WASP-43, HAT-P-20 and Qatar-2. *A&A*601:A53
- Fabrycky D Tremaine S (2007) Shrinking Binary and Planetary Orbits by Kozai Cycles with Tidal Friction. *ApJ*669:1298–1315
- Fabrycky DC Winn JN (2009) Exoplanetary Spin-Orbit Alignment: Results from the Ensemble of Rossiter-McLaughlin Observations. *ApJ*696:1230–1240
- Ford EB (2005) Quantifying the Uncertainty in the Orbits of Extrasolar Planets. *AJ*129:1706–1717
- Ford EB (2006) Improving the Efficiency of Markov Chain Monte Carlo for Analyzing the Orbits of Extrasolar Planets. *ApJ*642:505–522
- Gandolfi D, Collier Cameron A, Endl M et al. (2012) Doppler tomography of transiting exoplanets: a prograde, low-inclined orbit for the hot Jupiter CoRoT-11b. *A&A*543:L5
- Gaudi BS Winn JN (2007) Prospects for the Characterization and Confirmation of Transiting Exoplanets via the Rossiter-McLaughlin Effect. *ApJ*655:550–563

- Gaudi BS, Stassun KG, Collins KA et al. (2017) A giant planet undergoing extreme-ultraviolet irradiation by its hot massive-star host. *Nature*546:514–518
- Gillon M, Jehin E, Lederer SM et al. (2016) Temperate Earth-sized planets transiting a nearby ultracool dwarf star. *Nature*533:221–224
- Gillon M, Triaud AHMJ, Demory BO et al. (2017) Seven temperate terrestrial planets around the nearby ultracool dwarf star TRAPPIST-1. *Nature*542:456–460
- Giménez A (2006a) Equations for the analysis of the light curves of extra-solar planetary transits. *A&A*450:1231–1237
- Giménez A (2006b) Equations for the Analysis of the Rossiter-McLaughlin Effect in Extrasolar Planetary Transits. *ApJ*650:408–413
- Gizon L, Solanki SK (2003) Determining the Inclination of the Rotation Axis of a Sun-like Star. *ApJ*589:1009–1019
- Goldreich P, Tremaine S (1980) Disk-satellite interactions. *ApJ*241:425–441
- Greaves JS, Kennedy GM, Thureau N et al. (2014) Alignment in star-debris disc systems seen by Herschel. *MNRAS*438:L31–L35
- Guillochon J, Ramirez-Ruiz E, Lin D (2011) Consequences of the Ejection and Disruption of Giant Planets. *ApJ*732:74
- Hale A (1994) Orbital coplanarity in solar-type binary systems: Implications for planetary system formation and detection. *AJ*107:306–332
- Hébrard G, Bouchy F, Pont F et al. (2008) Misaligned spin-orbit in the XO-3 planetary system? *A&A*488:763–770
- Hébrard G, Désert JM, Díaz RF et al. (2010) Observation of the full 12-hour-long transit of the exoplanet HD 80606b. Warm-Spitzer photometry and SOPHIE spectroscopy. *A&A*516:A95
- Hébrard G, Ehrenreich D, Bouchy F et al. (2011a) The retrograde orbit of the HAT-P-6b exoplanet. *A&A*527:L11
- Hébrard G, Evans TM, Alonso R et al. (2011b) Transiting exoplanets from the CoRoT space mission. XVIII. CoRoT-18b: a massive hot Jupiter on a prograde, nearly aligned orbit. *A&A*533:A130
- Hellier C, Anderson DR, Collier-Cameron A et al. (2011) On the Orbit of the Short-period Exoplanet WASP-19b. *ApJ*730:L31
- Hirano T, Narita N, Shporer A et al. (2011a) A Possible Tilted Orbit of the Super-Neptune HAT-P-11b. *PASJ*63:531–536
- Hirano T, Suto Y, Winn JN et al. (2011b) Improved Modeling of the Rossiter-McLaughlin Effect for Transiting Exoplanets. *ApJ*742:69
- Holt JR (1893) Spectroscopic determination of stellar rotation. *Astro-Physics* XII:646
- Hosokawa Y (1953) On the Rotation Effect of Velocity Curves in Eclipsing Binary Systems. *PASJ*5:88
- Huang C, Wu Y, Triaud AHMJ (2016) Warm Jupiters Are Less Lonely than Hot Jupiters: Close Neighbors. *ApJ*825:98
- Huber D, Carter JA, Barbieri M et al. (2013) Stellar Spin-Orbit Misalignment in a Multiplanet System. *Science* 342:331–334
- Jensen ELN, Akeson R (2014) Misaligned protoplanetary disks in a young binary star system. *Nature*511:567–569
- Johnson JA, Winn JN, Albrecht S et al. (2009) A Third Exoplanetary System with Misaligned Orbital and Stellar Spin Axes. *PASP*121:1104
- Johnson MC, Cochran WD, Albrecht S et al. (2014) A Misaligned Prograde Orbit for Kepler-13 Ab via Doppler Tomography. *ApJ*790:30
- Johnson MC, Cochran WD, Collier Cameron A, Bayliss D (2015) Measurement of the Nodal Precession of WASP-33 b via Doppler Tomography. *ApJ*810:L23
- Kennedy GM, Wyatt MC, Sibthorpe B et al. (2012) 99 Herculis: host to a circumbinary polar-ring debris disc. *MNRAS*421:2264–2276
- Kopal Z (1942) The Calculation of Rotation Factors for Eclipsing Binary Systems. *Proceedings of the National Academy of Science* 28:133–140
- Kopal Z (1959) Close binary systems

- Kopal Z (ed) (1979) *Language of the stars: A discourse on the theory of the light changes of eclipsing variables*, Astrophysics and Space Science Library, vol 77, DOI 10.1007/978-94-009-9466-9
- Kostov VB, McCullough PR, Carter JA et al. (2014) Kepler-413b: A Slightly Misaligned, Neptune-size Transiting Circumbinary Planet. *ApJ*784:14
- Lai D (2014) Star-disc-binary interactions in protoplanetary disc systems and primordial spin-orbit misalignments. *MNRAS*440:3532–3544
- Lai D, Foucart F Lin DNC (2011) Evolution of spin direction of accreting magnetic protostars and spin-orbit misalignment in exoplanetary systems. *MNRAS*412:2790–2798
- Le Bouquin JB, Absil O, Benisty M et al. (2009) The spin-orbit alignment of the Fomalhaut planetary system probed by optical long baseline interferometry. *A&A*498:L41–L44
- Lendl M, Triaud AHMJ, Anderson DR et al. (2014) WASP-117b: a 10-day-period Saturn in an eccentric and misaligned orbit. *A&A*568:A81
- Lin DNC, Bodenheimer P Richardson DC (1996) Orbital migration of the planetary companion of 51 Pegasi to its present location. *Nature*380:606–607
- López-Morales M, Triaud AHMJ, Rodler F et al. (2014) Rossiter-McLaughlin Observations of 55 Cnc e. *ApJ*792:L31
- Louden T Wheatley PJ (2015) Spatially Resolved Eastward Winds and Rotation of HD 189733b. *ApJ*814:L24
- Madhusudhan N, Mousis O, Johnson TV Lunine JI (2011) Carbon-rich Giant Planets: Atmospheric Chemistry, Thermal Inversions, Spectra, and Formation Conditions. *ApJ*743:191
- Madhusudhan N, Bitsch B, Johansen A Eriksson L (2017) Atmospheric signatures of giant exoplanet formation by pebble accretion. *MNRAS*469:4102–4115
- Malmberg D, Davies MB Hogg DC (2011) The effects of fly-bys on planetary systems. *MNRAS*411:859–877
- Mamajek EE Hillenbrand LA (2008) Improved Age Estimation for Solar-Type Dwarfs Using Activity-Rotation Diagnostics. *ApJ*687:1264–1293
- Mancini L, Southworth J, Ciceri S et al. (2014) Physical properties, star-spot activity, orbital obliquity and transmission spectrum of the Qatar-2 planetary system from multicolour photometry. *MNRAS*443:2391–2409
- Marsh TR Horne K (1988) Images of accretion discs. II - Doppler tomography. *MNRAS*235:269–286
- Martin DV Triaud AHMJ (2014) Planets transiting non-eclipsing binaries. *A&A*570:A91
- Masuda K (2015) Spin-Orbit Angles of Kepler-13Ab and HAT-P-7b from Gravity-darkened Transit Light Curves. *ApJ*805:28
- Mayor M Queloz D (1995) A Jupiter-mass companion to a solar-type star. *Nature*378:355–359
- Mazeh T, Perets HB, McQuillan A Goldstein ES (2015) Photometric Amplitude Distribution of Stellar Rotation of KOIs - Indication for Spin-Orbit Alignment of Cool Stars and High Obliquity for Hot Stars. *ApJ*801:3
- McLaughlin DB (1924) Some results of a spectrographic study of the Algol system. *ApJ*60:22–31
- Molaro P, Monaco L, Barbieri M Zaggia S (2013) Detection of the Rossiter-McLaughlin effect in the 2012 June 6 Venus transit. *MNRAS*429:L79–L83
- Moutou C, Hébrard G, Bouchy F et al. (2009) Photometric and spectroscopic detection of the primary transit of the 111-day-period planet HD 80 606 b. *A&A*498:L5–L8
- Močnik T, Clark BJM, Anderson DR, Hellier C Brown DJA (2016) Starspots on WASP-85. *AJ*151:150
- Nagasawa M, Ida S Bessho T (2008) Formation of Hot Planets by a Combination of Planet Scattering, Tidal Circularization, and the Kozai Mechanism. *ApJ*678:498–508
- Naoz S, Farr WM, Lithwick Y, Rasio FA Teyssandier J (2011) Hot Jupiters from secular planet-planet interactions. *Nature*473:187–189
- Naoz S, Farr WM Rasio FA (2012) On the Formation of Hot Jupiters in Stellar Binaries. *ApJ*754:L36
- Narita N, Sato B, Hirano T Tamura M (2009) First Evidence of a Retrograde Orbit of a Transiting Exoplanet HAT-P-7b. *PASJ*61:L35–L40



- Neveu-VanMalle M, Queloz D, Anderson DR et al. (2016) Hot Jupiters with relatives: discovery of additional planets in orbit around WASP-41 and WASP-47. *A&A*586:A93
- Nikolov N Sainsbury-Martinez F (2015) Radial Velocity Eclipse Mapping of Exoplanets. *ApJ*808:57
- Nutzman PA, Fabrycky DC Fortney JJ (2011) Using Star Spots to Measure the Spin-orbit Alignment of Transiting Planets. *ApJ*740:L10
- Öberg KI, Murray-Clay R Bergin EA (2011) The Effects of Snowlines on C/O in Planetary Atmospheres. *ApJ*743:L16
- Ohta Y, Taruya A Suto Y (2005) The Rossiter-McLaughlin Effect and Analytic Radial Velocity Curves for Transiting Extrasolar Planetary Systems. *ApJ*622:1118–1135
- Oshagh M, Boisse I, Boué G et al. (2013) SOAP-T: a tool to study the light curve and radial velocity of a system with a transiting planet and a rotating spotted star. *A&A*549:A35
- Oshagh M, Dreizler S, Santos NC, Figueira P Reiniers A (2016) Can stellar activity make a planet seem misaligned? *A&A*593:A25
- Perryman M, Hartman J, Bakos GÁ Lindegren L (2014) Astrometric Exoplanet Detection with Gaia. *ApJ*797:14
- Petrie RM (1938) The Rotation Effect in Eclipsing Binaries and Stellar Dimensions. *JRASC*32:257
- Petrovich C (2015a) Hot Jupiters from Coplanar High-eccentricity Migration. *ApJ*805:75
- Petrovich C (2015b) Steady-state Planet Migration by the Kozai-Lidov Mechanism in Stellar Binaries. *ApJ*799:27
- Pont F, Gilliland RL, Moutou C et al. (2007) Hubble Space Telescope time-series photometry of the planetary transit of HD 189733: no moon, no rings, starspots. *A&A*476:1347–1355
- Queloz D, Eggenberger A, Mayor M et al. (2000) Detection of a spectroscopic transit by the planet orbiting the star HD209458. *A&A*359:L13–L17
- Queloz D, Anderson D, Collier Cameron A et al. (2010) WASP-8b: a retrograde transiting planet in a multiple system. *A&A*517:L1
- Rafikov RR (2006) Atmospheres of Protoplanetary Cores: Critical Mass for Nucleated Instability. *ApJ*648:666–682
- Rasio FA Ford EB (1996) Dynamical instabilities and the formation of extrasolar planetary systems. *Science* 274:954–956
- Rauer H, Catala C, Aerts C et al. (2014) The PLATO 2.0 mission. *Experimental Astronomy* 38:249–330
- Reiniers A, Lemke U, Bauer F, Beeck B Huke P (2016) Radial velocity observations of the 2015 Mar. 20 eclipse. A benchmark Rossiter-McLaughlin curve with zero free parameters. *A&A*595:A26
- Richards MT, Albright GE Bowles LM (1995) Doppler tomography of the gas stream in short-period Algol binaries. *ApJ*438:L103–L106
- Richards MT, Cocking AS, Fisher JG Conover MJ (2014) Images of Gravitational and Magnetic Phenomena Derived from Two-dimensional Back-projection Doppler Tomography of Interacting Binary Stars. *ApJ*795:160
- Rodler F, Lopez-Morales M Ribas I (2012) Weighing the Non-transiting Hot Jupiter  $\tau$  Boo b. *ApJ*753:L25
- Rogers TM, Lin DNC, McElwaine JN Lau HHB (2013) Internal Gravity Waves in Massive Stars: Angular Momentum Transport. *ApJ*772:21
- Rossiter RA (1924) On the detection of an effect of rotation during eclipse in the velocity of the brighter component of beta Lyrae, and on the constancy of velocity of this system. *ApJ*60:15–21
- Sahlmann J, Lovis C, Queloz D Ségransan D (2011) HD 5388 b is a  $69 M_{Jup}$  companion instead of a planet. *A&A*528:L8
- Sahlmann J, Triaud AHMJ Martin DV (2015) Gaia’s potential for the discovery of circumbinary planets. *MNRAS*447:287–297
- Sanchis-Ojeda R Winn JN (2011) Starspots, Spin-Orbit Misalignment, and Active Latitudes in the HAT-P-11 Exoplanetary System. *ApJ*743:61
- Sanchis-Ojeda R, Winn JN, Holman MJ et al. (2011) Starspots and Spin-orbit Alignment in the WASP-4 Exoplanetary System. *ApJ*733:127

- Sanchis-Ojeda R, Fabrycky DC, Winn JN et al. (2012) Alignment of the stellar spin with the orbits of a three-planet system. *Nature*487:449–453
- Santerne A, Moutou C, Tsantaki M et al. (2016) SOPHIE velocimetry of Kepler transit candidates. XVII. The physical properties of giant exoplanets within 400 days of period. *A&A*587:A64
- Schlaufman KC (2010) Evidence of Possible Spin-orbit Misalignment Along the Line of Sight in Transiting Exoplanet Systems. *ApJ*719:602–611
- Schlesinger F (1910) The Algol-variable [ $\delta$ ] Librae. *Publications of the Allegheny Observatory of the University of Pittsburgh* 1:123–134
- Schneider J (1994) On the occultations of a binary star by a circum-orbiting dark companion. *Planet Space Sci*42:539–544
- Seager S Deming D (2010) Exoplanet Atmospheres. *ARA&A*48:631–672
- Shporer A Brown T (2011) The Impact of the Convective Blueshift Effect on Spectroscopic Planetary Transits. *ApJ*733:30
- Snellen IAG (2004) A new method for probing the atmospheres of transiting exoplanets. *MNRAS*353:L1–L6
- Snellen IAG, de Kok RJ, de Mooij EJW Albrecht S (2010) The orbital motion, absolute mass and high-altitude winds of exoplanet HD209458b. *Nature*465:1049–1051
- Snellen IAG, Brandl BR, de Kok RJ et al. (2014) Fast spin of the young extrasolar planet  $\beta$  Pictoris b. *Nature*509:63–65
- Southworth J (2011) Homogeneous studies of transiting extrasolar planets - IV. Thirty systems with space-based light curves. *MNRAS*417:2166–2196
- Sullivan PW, Winn JN, Berta-Thompson ZK et al. (2015) The Transiting Exoplanet Survey Satellite: Simulations of Planet Detections and Astrophysical False Positives. *ApJ*809:77
- Szabó GM, Szabó R, Benkő JM et al. (2011) Asymmetric Transit Curves as Indication of Orbital Obliquity: Clues from the Late-type Dwarf Companion in KOI-13. *ApJ*736:L4
- Temple LY, Hellier C, Albrow MD et al. (2017) WASP-167b/KELT-13b: Joint discovery of a hot Jupiter transiting a rapidly-rotating FIV star. *ArXiv e-prints*
- Terquem C (2013) The effects of disc warping on the inclination of planetary orbits. *MNRAS*435:798–808
- Terquem C Ajmia A (2010) Eccentricity pumping of a planet on an inclined orbit by a disc. *MNRAS*404:409–414
- Triaud A (2016) Exoplanets: Migration of giants. *Nature*537:496–497
- Triaud AHMJ (2011a) Constraints on planetary formation from the discovery & study of transiting Extrasolar Planets. PhD thesis, Observatoire Astronomique de l'Université de Genève, <http://archive-ouverte.unige.ch/unige:18065>
- Triaud AHMJ (2011b) The time dependence of hot Jupiters' orbital inclinations. *A&A*534:L6
- Triaud AHMJ (2014) Colour-magnitude diagrams of transiting Exoplanets - I. Systems with parallaxes. *MNRAS*439:L61–L64
- Triaud AHMJ, Queloz D, Bouchy F et al. (2009) The Rossiter-McLaughlin effect of CoRoT-3b and HD 189733b. *A&A*506:377–384
- Triaud AHMJ, Collier Cameron A, Queloz D et al. (2010) Spin-orbit angle measurements for six southern transiting planets. New insights into the dynamical origins of hot Jupiters. *A&A*524:A25
- Triaud AHMJ, Queloz D, Hellier C et al. (2011) WASP-23b: a transiting hot Jupiter around a K dwarf and its Rossiter-McLaughlin effect. *A&A*531:A24
- Triaud AHMJ, Hebb L, Anderson DR et al. (2013) The EBLM project. I. Physical and orbital parameters, including spin-orbit angles, of two low-mass eclipsing binaries on opposite sides of the brown dwarf limit. *A&A*549:A18
- Triaud AHMJ, Gillon M, Ehrenreich D et al. (2015) WASP-80b has a dayside within the T-dwarf range. *MNRAS*450:2279–2290
- Triaud AHMJ, Martin DV, Ségransan D et al. (2017a) The EBLM Project IV. Spectroscopic orbits of over 100 eclipsing M dwarfs masquerading as transiting hot-Jupiters. *ArXiv e-prints*
- Triaud AHMJ, Neveu-VanMalle M, Lendl M et al. (2017b) Peculiar architectures for the WASP-53 and WASP-81 planet-hosting systems\*. *MNRAS*467:1714–1733

- Van Eylen V, Lund MN, Silva Aguirre V et al. (2014) What Asteroseismology can do for Exoplanets: Kepler-410A b is a Small Neptune around a Bright Star, in an Eccentric Orbit Consistent with Low Obliquity. *ApJ*782:14
- Ward WR (1997) Protoplanet Migration by Nebula Tides. *Icarus*126:261–281
- Watson CA, Littlefair SP, Diamond C et al. (2011) On the alignment of debris discs and their host stars' rotation axis - implications for spin-orbit misalignment in exoplanetary systems. *MNRAS*413:L71–L75
- Winn JN Fabrycky DC (2015) The Occurrence and Architecture of Exoplanetary Systems. *ARA&A*53:409–447
- Winn JN, Hamilton CM, Herbst WJ et al. (2006) The Orbit and Occultations of KH 15D. *ApJ*644:510–524
- Winn JN, Johnson JA, Albrecht S et al. (2009) HAT-P-7: A Retrograde or Polar Orbit, and a Third Body. *ApJ*703:L99–L103
- Winn JN, Fabrycky D, Albrecht S Johnson JA (2010a) Hot Stars with Hot Jupiters Have High Obliquities. *ApJ*718:L145–L149
- Winn JN, Johnson JA, Howard AW et al. (2010b) The Oblique Orbit of the Super-Neptune HAT-P-11b. *ApJ*723:L223–L227
- Winn JN, Albrecht S, Johnson JA et al. (2011) Spin-Orbit Alignment for the Circumbinary Planet Host Kepler-16 A. *ApJ*741:L1
- Wittenmyer RA, Welsh WF, Orosz JA et al. (2005) System Parameters of the Transiting Extrasolar Planet HD 209458b. *ApJ*632:1157–1167
- Wood PL, Maxted PFL, Smalley B Iro N (2011) Transmission spectroscopy of the sodium 'D' doublet in WASP-17b with the VLT. *MNRAS*412:2376–2382
- Wu Y Lithwick Y (2011) Secular Chaos and the Production of Hot Jupiters. *ApJ*735:109
- Wu Y, Murray NW Ramsahai JM (2007) Hot Jupiters in Binary Star Systems. *ApJ*670:820–825
- Wytenbach A, Lovis C, Ehrenreich D et al. (2017) Hot Exoplanet Atmospheres Resolved with Transit Spectroscopy (HEARTS). I. Detection of hot neutral sodium at high altitudes on WASP-49b. *A&A*602:A36
- Yan F, Fosbury RAE, Petr-Gotzens MG, Pallé E Zhao G (2015) Using the Rossiter-McLaughlin Effect to Observe the Transmission Spectrum of Earth's Atmosphere. *ApJ*806:L23
- Zahn JP (1977) Tidal friction in close binary stars. *A&A*57:383–394
- Zhou G, Bayliss D, Hartman JD et al. (2015) A High Obliquity Orbit for the Hot-Jupiter HATS-14b Transiting a 5400K Star. *ApJ*814:L16
- Zhou G, Latham DW, Bieryla A et al. (2016a) Spin-orbit alignment for KELT-7b and HAT-P-56b via Doppler tomography with TRES. *MNRAS*460:3376–3383
- Zhou G, Rodriguez JE, Collins KA et al. (2016b) KELT-17b: A Hot-Jupiter Transiting an A-star in a Misaligned Orbit Detected with Doppler Tomography. *AJ*152:136
- Zhuang Q, Gao X Yu Q (2012) The Rossiter-McLaughlin Effect for Exomoons or Binary Planets. *ApJ*758:111